Application of a bonded critical state model to design tunnel support for rockmass bulking

Ciantia, M. O.; Arroyo, M.; Kaiser, P.

Published in:
IOP Conference Series: Earth and Environmental Science

DOI:
10.1088/1755-1315/833/1/012162

Publication date:
2021

Application of a bonded critical state model to design tunnel support for rockmass bulking

M O Ciantia[1], M Arroyo[2] and P Kaiser[3]

[1]University of Dundee, United Kingdom;
[2]Universitat Politècnica de Catalunya, Spain;
[3]Laurentian University, Canada

m.o.ciantia@dundee.ac.uk

Abstract. Gabion-type support is a favoured option to restrain bulking in pillar walls of mine footprint tunnels. It uses closely spaced short reinforcements in tunnel walls (typically fully grouted rebar) in combination with surface support (rock fragment retention systems such as shotcrete, weld wire mesh, straps, etc.). The system is installed while the rock is still mostly intact and is conceived to maintain support capacity even when, the rock attains a fully fragmented state, acting then like a gabion or earth-reinforced type retaining wall. In this paper the interaction between the support system and the highly stressed pillar walls is investigated numerically by means of finite element analyses within the framework of displacement-based design. Because the material response should capture the passage from intact rock to fully fragmented state, an advanced elasto-plastic bonded constitutive model was adopted as a simulation framework. The model is calibrated to replicate the mechanical behaviour of Bursnip Sandstone and Amarelo Pais Granite. These two rocks were selected because of high quality triaxial tests results from the literature. After showing the good performance of the model to reproduce both low and high pressure triaxial compression behaviour an extensive parametric study investigating the effects of bolt types on gabion response is presented.

1. Introduction

Massive underground mining and particularly caving mines at deep levels (more than 1000m) is becoming ever more widespread. The development of cave mine infrastructure in such highly stressed environments may lead to excavation instability problems [1]. The way mine development sequencing and cave advance affect the re-distribution of induced stresses on mine infrastructure as mining progresses, needs to be considered for support design [2]. Rock support in burst-prone ground needs to resist large deformations due to rock "dilation", called bulking, during the violent failure of rock [1]. The term "bulking" is used to describe volume increases of the rockmass near an excavation due to geometric non-fit of fragments during the transition from competent to fractured and then to broken rock. Near excavations, bulking is unidirectional toward the excavation (perpendicular to the wall), a function of the applied tangential strain, and highly dependent on the confining stress. For this reason, gabbion-type support is a favoured option to restrain bulking in pillar walls of mine footprint tunnels. It uses closely spaced short reinforcements (typically fully grouted rebar) in combination with surface support (rock fragment retention systems such as shotcrete, weld wire mesh, straps, etc.). The system is installed while the rock is still mostly intact and is conceived to maintain support capacity even when, because of mining operations, the rock attains a fully fragmented state, acting then like a gabion or earth-reinforced type retaining wall.

The material response should capture the passage from intact rock to fully fragmented state to properly simulate typical bulking effects. Previous numerical simulations adopting a discontinuum approach [3] where able to reproduce the typically observed unidirectional bulking of massive rockmasses around tunnels. Nevertheless, such discrete approaches are computationally very expensive if implemented in large scale caving models. Also, the inclusion of structural elements, such as elastoplastic bolts, adds further complexity to that approach.

In this paper an advanced elasto-plastic bonded constitutive model called herein "Cemented CASM" (C-CASM) and described by [4] has been used to simulate gabion-type support systems using a FE commercial FE package, PLAXIS [5]. The C-CASM model was implemented as a user defined model in PLAXIS allowing for the use of the several tools to represent structural reinforcements for geotechnical purposes. In what follows, after a brief overview of C-CASM, the model is calibrated to capture typical Sandstone and Granite behaviour. The calibrated model is then used for an extensive parametric analysis considering various types of reinforcement.

2. The constitutive model

Gens and Nova [6] introduced the conceptual bases for the extension of the classical theory of plasticity to incorporate the effects of bonding – cementation. Introducing an additional set of 'bonding-related' internal variables and describing the mechanical bond degradation by means of suitable hardening rules Gens and Nova showed how the critical state soil mechanics framework could be used to quantitatively describe the mechanical effects of hard soils and soft rocks. Since then several constitute models developed based on this original approach. For example, [7] showed the C-CASM to model cemented clays whilst more recently [8,9] showed how a large strain formulation of a similar models can be used to simulate CPT in structured clays and soft rocks respectively. In this work the cemented clay and sand model (C-CASM) fully described in [4] is used. In the model, the size of the yield locus (figure 1a) is controlled by the level of bonding (b). The shape of the yield locus is the same of the hypothetical uncemented rock and its evolution is controlled by the variables p'_c and p'_t, which control respectively the isotropic compression yield and the tensile yield of the material. These intermediate variables are:

$$p'_c = p'_s(1+b) \text{ and } p'_t = p'_s(\alpha b) \tag{1}$$

where, p'_s is the equivalent pre-consolidation pressure of the corresponding uncemented material for each current state; α is a parameter associated to tensile strength directly depending on the cementation. The yield surface is then expressed by,

$$f = \left(\frac{q}{M\left(p' + p'_t\right)} \right)^n + \frac{1}{\ln r} \ln \left(\frac{p' + p'_t}{p' + p'_c} \right) \tag{2}$$

where M is the stress-ratio (q/p') at critical state and, n and r are model parameters controlling the shape of yield surface. Bonding evolution is defined by the following exponential law,

$$b = b_0 \, \mathrm{e}^{-(h-h_0)} \tag{3}$$

$$dh = h_1 \left| d\varepsilon_v^p \right| + h_2 \left| d\varepsilon_s^p \right| \tag{4}$$

where h_1 and h_2 are material parameters (greater than zero) defining the degradation rate resulting from volumetric and shear strains, respectively; h_0 represents a limit degradation, usually null; and b_0 is the initial bonding. Following [10] the elastic stiffness for cemented materials is made dependent on bonding, this implies a state-dependent elastic bulk modulus and, in turn, a Young modulus given by

$$E_c = 3(1-2\upsilon)K_c = 3(1-2\upsilon)\frac{\upsilon p'}{\kappa}\left(1+\sqrt{\frac{p_s b}{p'}}\right) \tag{5}$$

A major consideration in selecting a material model for practical applications is that of economy of description. The behaviour sought-after should be described with as few parameters as possible. The C-CASM has 11 parameters easily calibrated as shown in [11].

3. Constitutive model calibration

The model is calibrated to reproduce the behaviour of a Sandstone and a Granite in an effort to showcase the model's capability of reproducing rock behaviour. The low confinement triaxial tests on Bursnip's Road sandstone reported by [12] and the high pressure triaxial test on Berea sandstone by [13] were used for the sandstone calibration (figure 1a). On the other hand, the Amarelo Pais Granite, for which a high-quality database of triaxial tests is found in the literature [14], was chosen as representative for a very low porosity rock behaviour. Ref. [14] included ample information about the yield points of this and similar granites (figure 1b), but not much in terms of volumetric compression.

In general, the experiments on these two rocks types indicate a distinctive pattern of dilatancy evolution. A model parametric analysis was performed to identify which parameters had more bearing on dilatancy evolution. Figure 1 shows the final calibrated model performance against the experimental data and table 1 summarises the calibrated model parameters for both rocks. The ability of the model to capture the curved yield locus and the brittle-dilatant response of the rock is key. Such features, that an elasto-perfectly plastic model such as Mohr-Coulomb would fail to reproduce, control stress redistributions, the failure mechanism and consequently, as detailed in the next section, the loading of tunnel support.

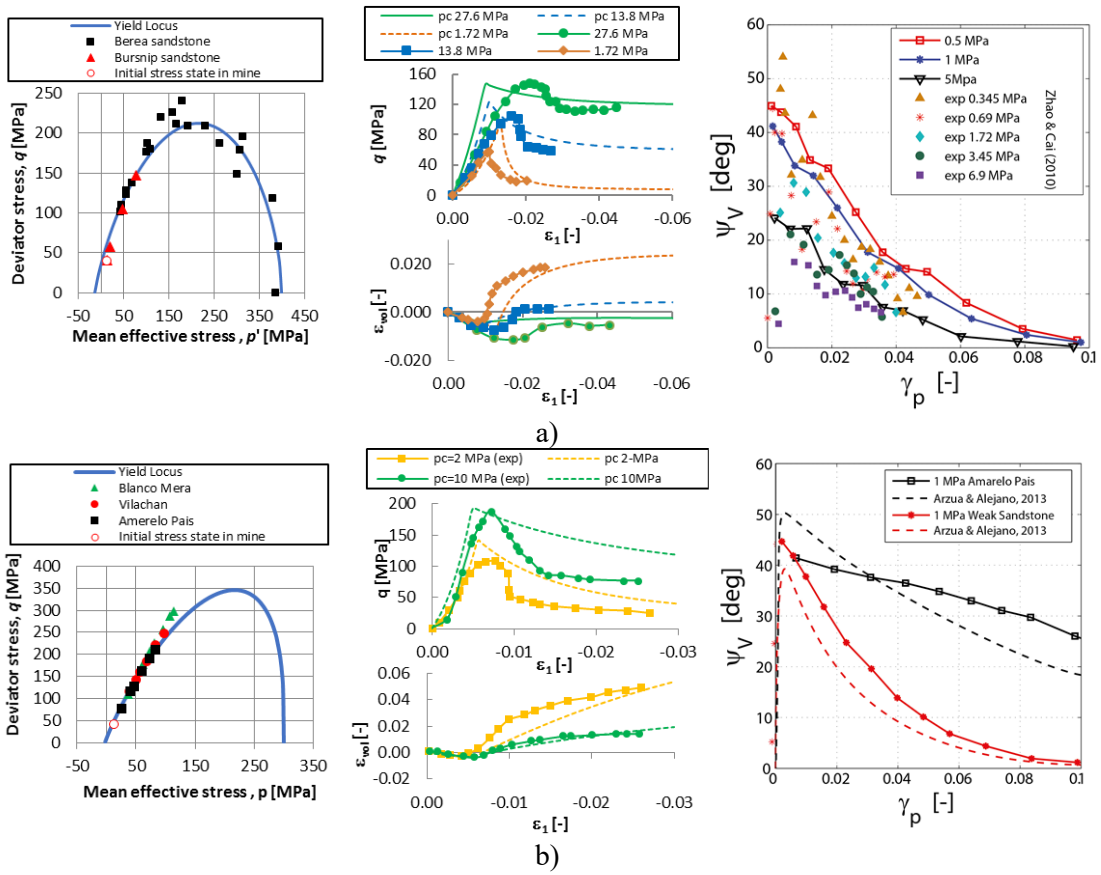

Figure 1. Model calibration for Sandstone (a) and Granite (b). Yield locus (left) stress strain response for selected triaxial tests (centre) and dilatancy vs invariant measure of incremental shear plastic strain for plane strain condition (right).

Table 1. Calibrated model parameters and internal variables initial conditions.

Material	ν	λ	κ	h_1	h_2	M	n	r	α_t	p_c' (MPa)	b_0	β
Bursnip sandstone	0.25	0.03	0.019	5	2.5	1.2	1.7	2.5	0.05	400	3	0.6
Amarelo Granite	0.17	0.067	0.0067	10	5	1.2	3.1	1.15	0.02	300	1	0.7

4. Tunnel support modelling

Mining-induced stress changes can cause an expansion of the yield zone surrounding a tunnel with a related change in confinement (σ_3). As a result, the tunnel and the rockmass surrounding the tunnel are further deformed (after excavation). The image on the left in figure 2 shows an example of tangential straining of the drift wall due to roof sag or floor heave. When excessively strained and stressed or relaxed, excavations may experience a high risk of dynamic failure [1]. Bulking deformations hence dominate the support behaviour, and support in a bulking ground should be selected considering deformation-based design principles [15,16]. Stiff and brittle support rings of limited capacity, if installed before the mining-induced bulking occurs, may suddenly fail due to bulking of stress-fractured ground behind the support or inside the supported rockmass. A reinforced rockmass may "burst" even if the rockmass is not loaded by a dynamic disturbance. A 5 by 5 m mine rib pillar is considered to numerically model the impact of tangential straining.

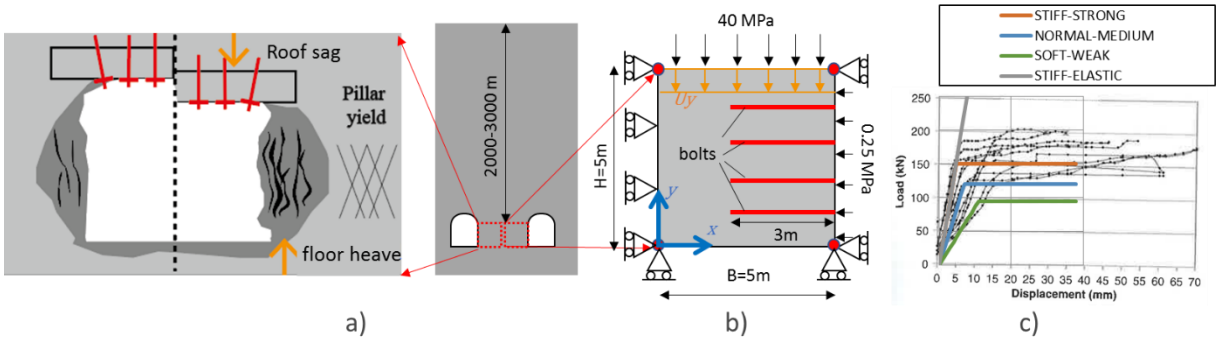

Figure 2. a) Deep mine tunnel configuration including the illustration of mining-induced tangential straining of drift wall due to floor heave or roof sag (roof loading or pillar yield) adapted from [2], b) FEM model geometry and boundary conditions and c) bolt typology analysed against pull-out tests done in the field at LaRonde on hybrid bolts [17].

The geometry of the FEM model is represented in figure 2 and, to simulate the mechanical behaviour of a deep mine pillar within the framework of displacement-based design, the simulation is subdivided in three steps:

1. Stress initialization: An initial vertical stress of 40 MPa is imposed to the top boundary of the FEM model. This value is considered broadly representative of deep mining conditions. The lateral confinement is zero, to simulate the presence of the gallery. This initial stress level is also represented in the calibrated yield locus of the two rock types in figure 1.
2. Activation of reinforcement: This always includes bolting which is always represented by embedded plates. Tunnel face shotcrete was represented as an internal face pressure of 0.25 MPa.
3. Imposition of a "tangential" strain to the rock by applying a vertical uniform displacement to the top boundary of the FE model.

The rock reinforcement considered here includes a square pattern of grouted bolts and shotcrete/wired mesh face support. The hypothesis and procedures followed to represent this reinforcement follow the indications on PLAXIS software manual [5]. The principle is to assign a strength and a stiffness per unit depth. Axial and flexural stiffness will hence change depending on the number of bolts represented per unit meter depth.

Table 2. Mechanical and geometrical properties of the different generic types of bolts.

Bolt description	S_h [m]	E_{eq} [GPa]	EA [MN/m]	EI [kN/m]	N_p [kN/m]	M_p[kNm/m]
STIFF-STRONG	1	54	65	6	150	5
NORMAL-MEDIUM	1	43	32	2	120	5
SOFT-WEAK	1	36	16	1	90	5
STIFF - ELASTIC	1	54	65	6	-	-

The bolts are always 3 m long with a 1 m vertical spacing. Their stiffness and strength are variable, reflecting different horizontal spacing between bolts as well as single-bolt characteristics (figure 2). Table 2 summarizes the mechanical characteristics with which different bolting patterns have been represented in the simulation. The bolt description for each type is representative of their stiffness-strength levels and also includes a number indicating the assumed number of bolts per longitudinal meter (except when a single bolt per meter is assumed, when no number is indicated). The main simulation series considered the effect of different bolt types on the gabion response for both sandstone and granite rocks. Complementary studies on some modelling aspects such as the effect of different case support, tangential strain definition and the timing of bolt activation were also performed but are not be presented here.

5. Results

Figure 3 illustrates the Gabion load bearing capacity for the Sandstone. A similar but stiffer response was obtained for the granite material. Macro-scale results presented in figure 3 show that, in general, the pillar wall capacity was moderately enhanced (15%) by bolting and that bolting resulted in a more ductile response. However, when bolting used stiff-strong bolts the general trend was broken, and the pillar wall was weaker and less ductile than when other bolts were used.

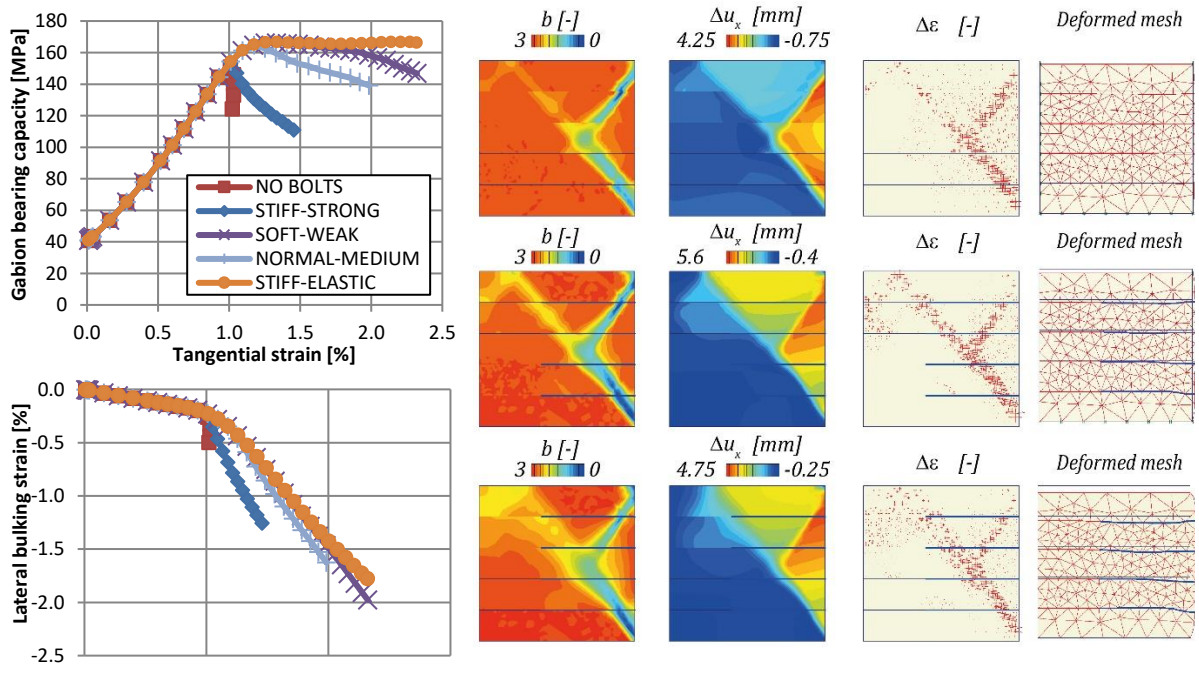

a) b)

Figure 3. a) Effect of bolt type on gabion load (top) and lateral bulking strain (bottom). b) From left to right bonding related variable evolution, incremental horizontal displacement, principal incremental strains and deformed mesh at failure for FEM simulations characterized by (top row) no bolts, (middle row) STIFF-ELASTIC bolts and (bottom row) SOFT-WEAK bolts.

A detailed examination of the simulation results allows to understand the influence of bolt strength and stiffnes on the behaviour of the reinforced rockmass. Figure 3 presents a set of snapshots of the gabion at failure. The 3 sets of results from to bottom correspond to, no bolts, strong-stiff bolts and soft-weak bolts respectively. The main observations from these figures are:

1. A triangular rigid wedge develops at the face exposed to the free surface (right) for all cases. This is in part a result of the chosen constitutive model that simulates yield rather than extensional/spalling failure.

2. From the bottom-up the inner part of the rock is more damaged as yielding and bond degradation extend towards the internal part of the gabion. This means that the plastic resources of the material are also activated in the inner part of the gabion thanks to the presence of the bolts.
3. The more ductile response of the reinforcements using the softer/weaker bolts (stiff-elastic, soft-weak, normal-medium) is visible on from the deformed mesh plot, indicating larger displacements.

The fact that the rockmass with strong-stiff bolts fails at less load and in a more brittle manner deserves further investigation. To clarify this response, a detailed analysis of the two extreme cases of bolting (i.e stiff-strong and soft-weak) was performed. Figure 4 presents the findings regarding the stiff-strong bolts simulation. It is evident that in this case the bolts, being stiff, yield before the gabion structural response reaches the peak (at point B all bolts have already yielded). At that stage the rock plasticization is still very limited. At the peak pillar capacity (point C) the plastic wedge is incipient, but all the bolts are almost fully yielded. Post peak (D, E) the bolts start to unload as the immobile side of the gabion expands in elastic release while the broken wedge starts sliding. The bolts fail in shear failure due to localized shearing, a commonly observed failure mode for stiff rock bolts.

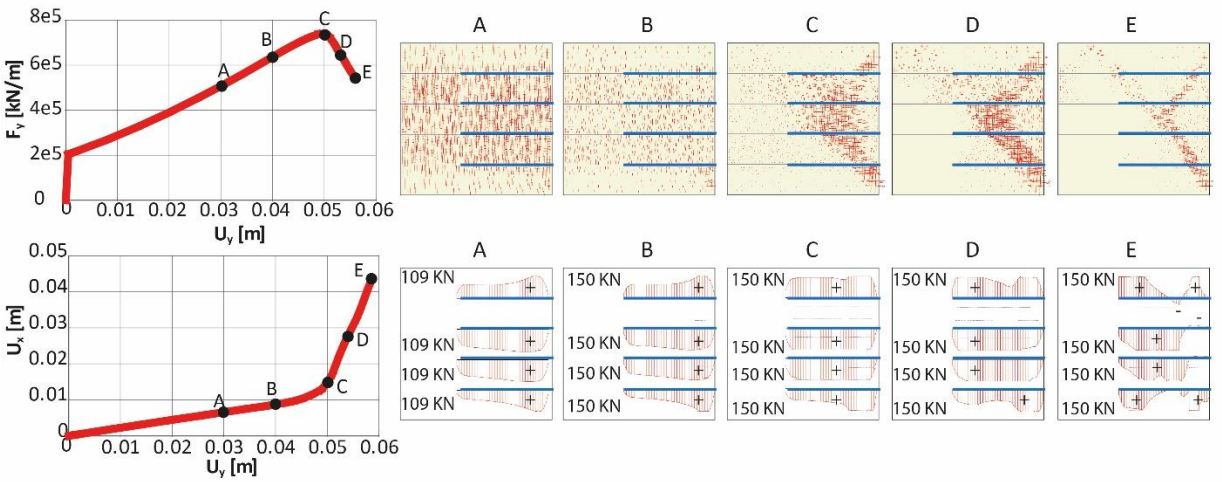

Figure 4. Detailed analysis of the STIFF-STRONG case. Snapshots of incremental principal strains and bolt axial load (positive when in tension) at 5 moments (A, B, C, D, E) of the simulation.

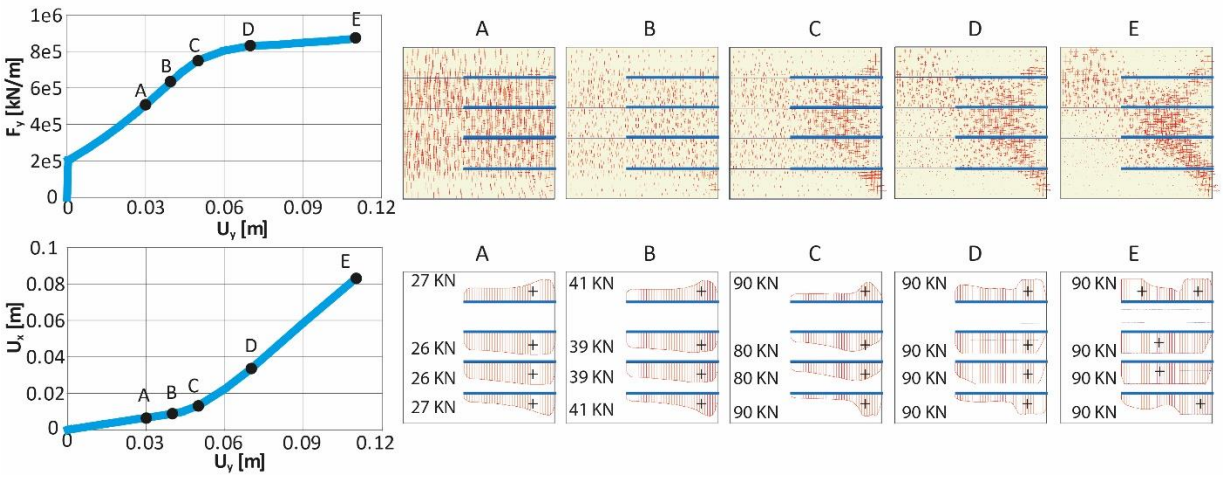

Figure 5. Detailed analysis of the SOFT-WEAK case. Snapshots of incremental principal strains and bolt axial load (positive when in tension) at 5 moments (A, B, C, D, E) of the simulation.

Similarly, figure 5 presents a detailed analysis of the gabion response with soft-weak bolting. Here, the bolts do not yield before the gabion does (points A, B). At gabion yield (point C) bolt yield is incipient. During wedge sliding (points D, E) there is still a reserve of strength in all the bolts that is progressively mobilized. Due to the bending and rotation of the bolts in the wider yield zone, the full tensile capacity of the bolts is mobilized. In this case, the bolt stiffness is better matched to that of the supported rock. A detailed inspection of the bolt deformation revealed that bolt straining is far from uniform and that stiffer bolts, despite having more capacity than the soft bolts, yield at less imposed tangential strain. It was also found that the deformation within the bolt coincides with the mean bulk strain only during the elastic deformation of the gabion. As soon as this condition is lost, and plastic deformation localizes into a wedge mechanism the gabion mean bulk strain becomes meaningless to predict the bolt response. From figure 6, it is evident how the stiff-strong bolts yield before than the soft-weak bolt. Moreover, in the strong-stiff case the deformation of the middle part of the bolt is such that it unloads until being compressed (and sheared; not shown).

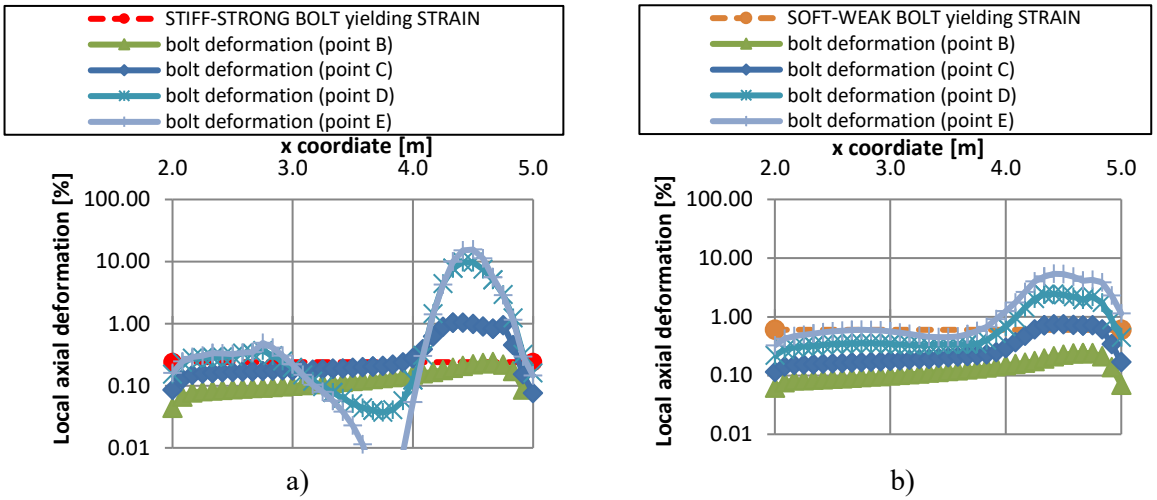

Figure 6. Local axial deformation as a function of the x coordinate of the bottom bolt at different levels of loading (B, C, D, E) for the a) STIFF-STRONG model and b) SOFT-WEAK model.

6. Conclusions

In this paper a generalized critical state model of the type represented by C-CASM is used to match rock behaviour. The stress-strain dependence of dilatancy is accommodated by the model. The calibration process is well constrained for high porosity rocks, i.e., for a compressible sandstone, for which a large amount of compression data is available. The inclusion of the "bonding" state variable in the model identifies shear localization damage patterns in the rock. This is in line with the approach of smeared fracture models that have been repeatedly applied to model concrete. A series of simulations have been performed to analyse several aspects of the reinforced rock response. The main conclusions are:

1. Whereas the reinforcement only marginally enhances the pillar's maximum capacity, it transforms the rocks behaviour to a far more ductile post-peak response. The stiffness of the reinforcement should be appropriately matched to that of the rock.
2. The more ductile response of the reinforcements using weaker and softer bolts is evident from the deformed mesh plot, indicating larger displacements.
3. The relative stiffness between the reinforcement and the rock is key as it governs the onset of bolt yield. If this happens when the gabion is still in the pre-peak (lightly damaged) conditions, then the failure mechanism is more brittle as the bolts fail prematurely.

From the numerical modelling viewpoint, a shortcoming of the current model formulation is that it does not include any kind of numerical stabilization to avoid mesh dependency. Future developments should extend the model so that at least roof and ceiling of the gallery are included. It is likely that the uniform tangential straining assumption would play a lesser role in enlarged models. Finally, 3D

simulations are highly recommended as, apart from dealing with more complex gallery-drawpoint geometries, they would allow to represent in a more straightforward manner the properties of bolted reinforcement.

Acknowledgments

This work was partly supported by the Ministry of Science and Innovation of Spain through the research grant BIA2017-84752-R

References

[1] Kaiser PK and Cai M 2012 Design of rock support system under rockburst condition. *J Rock Mech Geotech Eng*. **4** 215–27
[2] Kaiser PK 2018 Excavation Vulnerability and Selection of Effective Rock Support to Mitigate Rockburst Damage. *Rockburst Mech. Monit. Warn. Mitig.*, Elsevier Inc., p. 473–518.
[3] Garza-Cruz TV, Pierce M and Kaiser PK 2014. Use of 3DEC to study spalling and deformation associated with tunnelling at depth. In *Proceedings of the Seventh International Conference on Deep and High Stress Mining* (pp. 421-434). Australian Centre for Geomechanics.
[4] González NA, Arroyo M and Gens A 2009 Identification of bonded clay parameters in SBPM tests: A numerical study. *Soils Found*. **49** 329–40
[5] Brinkgreve RBJ, Kumarswamy S, Swolfs WM and Foria F. 2018 PLAXIS 2018.
[6] Gens A and Nova R 1993 Conceptual bases for a constitutive model for bonded soils and weak rocks. In: *Proc. Int. Conf. hard soils - soft rocks, vol. 1, Athens: Rotterdam : Balkema*. 485–94.
[7] Arroyo M, Ciantia M, Castellanza R, Gens A and Nova R. 2012 Simulation of cement-improved clay structures with a bonded elasto-plastic model: A practical approach. *Comput Geotech*. **45**:140–50.
[8] Hauser L and Schweiger HF 2021 Numerical study on undrained cone penetration in structured soil using G-PFEM. *Comput Geotech*. **133** 104061.
[9] Oliynyk K, Ciantia MO and Tamagnini C. 2021 A finite deformation multiplicative plasticity model with non – local hardening for bonded geomaterials. *Comput Geotech*. https://doi.org/10.1016/j.compgeo.2021.104209
[10] Yu HS, Tan SM and Schnaid F. 2007 A critical state framework for modelling bonded geomaterials. *Geomech Geoengin*. **2** 61–74
[11] Rios S, Ciantia M, Gonzalez N, Arroyo M and da Fonseca AV. 2016 Simplifying calibration of bonded elasto-plastic models. *Comput Geotech* **73**.
[12] Zhao XG and Cai M. 2010 A mobilized dilation angle model for rocks. *Int J Rock Mech Min Sci*; **47** 368–84
[13] Wong TF, Szeto H and Zhang J. 1992 Effect of loading path and porosity on the failure mode of porous rocks. *Appl Mech Rev*. **45** 281–93.
[14] Arzúa J, Alejano LR and Walton G. 2014 Strength and dilation of jointed granite specimens in servo-controlled triaxial tests. *Int J Rock Mech Min Sci* **69** 93–104.
[15] Kaiser PK and Moss A. 2021 Deformation-based support design for highly stressed ground with focus on Rockburst Damage Mitigation.*J Rock Mech Geotech Eng.* (Accepted)
[16] Kaiser PK. 2014 Deformation-based support selection for tunnels in strainburst-prone ground. Seventh Int. Conf. Deep High Stress Mining, 16-18 Sept. Sudbury, Australian Centre for Geomechanics; 2014, p. 227–40.
[17] Mercier-Langevin F, Turcotte P. Evolution of Ground Support Practices At Agnico-Eagle's LaRonde Division - Innovative Solutions to High-stress Yielding Ground. 1st Canada-US Rock Mech. Symp. Am. Rock Mech. Assoc., Vancouver: ARMA; 2007.